M. Burkow, M. Griebel

Numerical Simulation of the Temporal Evolution of a Three Dimensional Barchanoid Dune and the Corresponding Sediment Dynamics

Numerical Simulation of the Temporal Evolution of a Three Dimensional Barchanoid Dune and the Corresponding Sediment Dynamics

M. Burkow[a], M. Griebel[a,b]

[a]*Institute for Numerical Simulation, University of Bonn, Wegelerstrasse 6, 53115 Bonn, Germany*
[b]*Fraunhofer-Institut für Algorithmen und Wissenschaftliches Rechnen SCAI, Schloss Birlinghoven, 53754 Sankt Augustin, Germany*

Abstract

In this paper we present the results of the numerical simulation of a three-dimensional current-driven sediment transport process. In detail, the temporal evolution of a barchanoid dune is studied. Two phenomena are treated in this context. First, the three-dimensional flow of a single phase fluid is considered. Second, the interaction of the flow and the sediment bed with its morphological change of the sediment surface is taken into account. Here, we numerically solve the instationary incompressible Navier-Stokes equations. The morphological change of the sediment bed is modelled by Exner's bed level equation. Furthermore, the suspended material is treated as a sediment concentration and modelled by an advection-diffusion equation. Both models are discretised and explicitly coupled to the discrete fluid model. The typical sedimentary processes and the sedimentary form of a barchanoid dune are well captured by our numerical simulation.

Keywords: Numerical Simulation, Sediment Transport, Barchanoid Dune, CFD

1. Introduction

Sediment transport processes and their effects on the morphology of the sediment bed are significant issues in hydraulic engineering. Usually, the physical processes of the formation of dunes and other sedimentary forms are studied in laboratory flumes or in field experiments. These time-intensive and costly studies are not always easy to conduct. At this point, a numerical simulation can help to reduce costs and to provide more insight and therefore a better understanding of the relevant flow and transport phenomena.

There are different classifications of dunes in the aeolian regime as well as in the fluvial regime. For example, linear dunes, crescent shaped dunes, e.g. parabolic or barchanoid dunes, and star shaped dunes demonstrate the large diversity of dune forms. Here, the availability of sand, its consistency, the predominant wind situation and many other factors determine the dune type, compare Goudie (2014). In general, the sediment is transported in the bed load layer over the dune body upwards the luvslope. When the sand particles reach the top end of the dune, the particles slide down the leeslope, which is limited by the angle of repose. In case of a barchanoid dune, the transport velocities are higher near the lateral ends of the dune body. This fact leads to a faster transport of the sand at the sides of the dune body and to the development of sand horns, which

---

are transported further downstream. The resulting dune body and the involved processes are strictly three-dimensional. We present a numerical approach for their simulation and discuss the obtained results.

The remainder of this paper is organised as follows. In section two, we describe the full fluid-sediment-model, which consists of the Navier-Stokes equations, a suspension load model, and Exner's bed level equation. In section three, we shortly discuss our numerical discretisation and its properties. In section four, we present the results of our numerical simulation for the temporal evolution of a barchanoid dune. A conclusion is given in section five.

2. Model: Navier–Stokes & Sediment model

In the following the used model is presented. It consists of a three-dimensional fluid model and the sediment equations, which realise the suspension load transport and the morphological change of the sediment surface. Parts of the presented models were previously studied in the literature, e.g. Giri and Shimizu (2006), Kubatko et al. (2006), Kubatko and Westerink (2007), Khosronejad et al. (2012), Nabi et al. (2013), and Doré et al. (2016). Some authors already combined a two or three dimensional fluid solver with a sediment model for the morphological change (Kubatko et al. (2006), Kubatko and Westerink (2007), Burkow and Griebel (2016)) or the suspension load (Campos (2001), Nabi et al. (2013)).

In this chapter, we introduce a novel full three dimensional coupling algorithm for all three models.

2.1. Navier–Stokes equations

Due to the complex three-dimensional character of sedimentary bedforms and especially dunes, it is necessary to apply a full three-dimensional model. Here, the instationary incompressible Navier-Stokes equations in their dimensionless form read as

$$\frac{\partial \mathbf{u}}{\partial t} + \nabla \cdot (\mathbf{u} \otimes \mathbf{u}) = \frac{1}{Fr}\mathbf{g} - \nabla p + \frac{1}{Re}\Delta \mathbf{u}, \tag{1a}$$

$$\nabla \cdot \mathbf{u} = 0 \qquad\qquad \text{on} \quad \Omega_f \in \mathbb{R}^3, \tag{1b}$$

where $\mathbf{u}$ is the velocity, p is the pressure, $\mathbf{g}$ are the volume forces, and Ω_f denotes the domain of the fluid body. Moreover

$$Re = \frac{\mathbf{u}_\infty \cdot l}{\nu} \tag{2}$$

denotes the Reynolds number and

$$Fr = \frac{\mathbf{u}_\infty}{\sqrt{g \cdot l}} \tag{3}$$

denotes the Froude number. Both, Re as well as Fr, are dimensionless numbers which characterise the flow conditions. The characteristic length and velocity are denoted by l and $\mathbf{u}_\infty$, respectively. As usual, ν stands for the kinematic viscosity of the fluid.

In this study, we solely concentrate on the realisation of a fully coupled fluid sediment model. A qualitative comparison with an experimental work would require a turbulence

model. But there are several issues why there is no turbulence model applied in this paper. First, the suspended material would affect the turbulence structures. As far as we know no reliable model to reproduce this effect in a numerical simulation was available in the literature. Second, a turbulence model would need a wall model for the velocities, equally the suspension load is not regarded in the standard wall models. Third, the diffusion constant K would change in a turbulent regime. Here, a suitable model for the diffusion coefficient K was not available in the literature. All this considerations do not lead to a suitable choice of a turbulence approach and the related coefficients for the models. Thus, a direct numerical simulation is employed for the fluid model and further modeling approaches, e.g. turbulence models, are not taken into account.

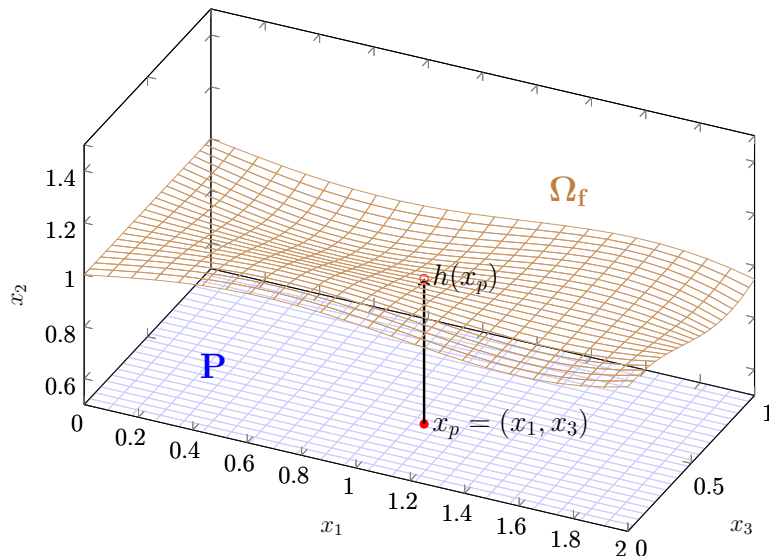## 2.2. Sediment surface and the Exner equation

Figure 1: The sediment surface is described for each time point t by its height $h(x_1, x_3)$, i.e. the distance from a underlying plane $P = (x_1, x_3)$. Thus, the fluid domain Ω_f is bounded by $h(x_1, x_3)$ from below.

The Navier–Stokes equations are solved on a time-dependent fluid domain Ω_f. The bottom of this domain is bounded for each time point by its sediment surface $h(x_1, x_3)$. This sediment surface h describes the height of the underlying sediment with respect to a reference plane $P = (x_1, x_3)$, compare Figure 1. To model the temporal change of the sediment surface h, we use the bed level equation postulated by Exner (1925), i.e.

$$\frac{\partial h}{\partial t} + \nabla_{(x_1, x_3)} \cdot \mathbf{q}_s(\tau(\mathbf{u})) = 0 \qquad \text{on } P, \qquad (4a)$$

$$\frac{\partial h}{\partial n} = 0 \qquad \text{on } \Gamma_P, \qquad (4b)$$

where $\mathbf{q}_s(\tau(\mathbf{u}))$ is the transport rate function of the sediment and the gradient operator with respect to (x_1, x_3) is denoted by $\nabla_{(x_1, x_3)}$. It depends on the shear stress τ, which is a function of the fluid velocity $\mathbf{u}$, where $\tau(\mathbf{u})$ is here just needed on the sediment surface. In the Neumann boundary condition (4b) the normal is denoted by n. The Exner equation states that the net balance between gain and loss of mass in a certain control volume results in a change of the sediment height h. It was sucessfully used in several studies to investigate the evolution of geomorphological change, e.g. Parker (2004), Paola and

3

Voller (2005), Kubatko et al. (2006), Kubatko and Westerink (2007). The presented model results from the conservation of mass and therefore from first principles. Moreover, Coleman and Nikora (2009) used a statistical averaging process of a granular bed over time and space to derive the Exner equation.

The sediment surface determined by h denotes implicitly the fluid domain Ω_f. Thus, a change in h results in a change of the fluid domain Ω_f. Several models for the shear stress $\tau : \mathbb{R}^3 \mapsto \mathbb{R}^2$ and the transport rate function $\mathbf{q}_s : \mathbb{R}^2 \mapsto \mathbb{R}^2$ are available in the literature, see Chanson (1999). In the following, we choose the empirically derived models (5a) and (5b)

$$\mathbf{q}_s = \sqrt{(s-1)gd_{50}^3} \cdot \left(\frac{4\tau(\mathbf{u})}{\rho_f(s-1)gd_{50}} - \tau_c \right)^{\frac{3}{2}}, \tag{5a}$$

$$\tau(\mathbf{u}) = \frac{1}{8} \rho_s f \left| \mathbf{u} \right|^2, \tag{5b}$$

where ρ_s denotes the sediment density, d_{50} is the median grain size, τ_c is the dimensionless critical shear stress and $s = \rho_s/\rho_f$ with ρ_f being the fluid density. The friction parameter is set according to Chanson (1999) as

$$f = \frac{64}{Re} \tag{6}$$

which is valid for flows with $Re < 2000$.

Chanson (1999) proposed formula (5b) as a modified version of the transport formula from Meyer-Peter and Müller (1948), which has been validated by numerous experimental studies. Wong and Parker (2006) gave a nice summary and analysis of (5a).

2.3. Suspension load model

The suspension load comprises all material which is transported in the whole fluid. An advection-diffusion model is used to describe the transport of the suspended material.

Since only very fine grains are transported, the common approach is to model the entrained material as a concentration c of mass in the fluid domain. Similar to the bed level equation, the advection-diffusion model for the suspended material can be derived from the conservation of mass and momentum. Malcherek (2004) presented a suspension model as

$$\frac{\partial c}{\partial t} + \mathbf{u} \cdot \nabla c + w_g \frac{\partial c}{\partial x_2} = K\Delta c \qquad c(\mathbf{x}, t) : \Omega_f \times [0 : T] \longrightarrow \mathbb{R}, \tag{7a}$$

$$\frac{\partial c}{\partial n} = 0 \qquad \mathbf{x} \in \Gamma_{\Omega_f}, \tag{7b}$$

$$c = c_{ref} \qquad \mathbf{x} \in \Gamma, \tag{7c}$$

where the fluid velocity is denoted by $\mathbf{u}$, the sediment surface is given by

$$\Omega_s := \{(x_1, h(x_1, x_3), x_3) \,|\, (x_1, x_3) \in P\}, \tag{8}$$

and the diffusion coefficient is described by K. Here, the values for K are typically very small. Officer (1982) deduced values of the size $10^{-7} \, m^2/s$ from experimental studies. To take the gravitational transport of particles into account a velocity w_g is added as an additional advection velocity component. On the one hand, the Neumann boundary

condition in equation (7b) models a closed boundary of the fluid domain Ω_f. On the other hand, the boundary condition at the sediment surface Ω_s reflects the idea that the layer next to the sediment body has a concentration c_{ref} which is the maximum concentration near Ω_s. This model and similar forms were used to model the transport and the diffusion of the suspended material in various applications and experimental approaches, compare Campos (2001), Marek (2001), Wu et al. (2005), Yoon and Kang (2005), Sedimentation & River Hydraulics Group (2006), Kantoush et al. (2008), Razmi et al. (2009), and James et al. (2010).

2.4. Gravitational component

In the advection-diffusion equation (7a) the settling of single particles and its impact on the transport is modelled by a velocity w_g which results from gravitational forces. Here, a particle is modelled as a falling sphere in a fluid. With Stokes' law as stated in Daintith (2009), a terminal velocity for fine spherical particles can be calculated from

$$w_g = \frac{(\rho_s - \rho_f)/\rho_f g d_s^2}{C_1 \nu}, \tag{9}$$

where ρ_f and ρ_s denote the material densities. The gravity, the viscosity, and the grain size are denoted by g, ν, and d_s. The theoretical constant $C_1 = 18$ is only valid for perfect spheres. Additionally, Stokes' law is only valid in the low Reynolds number regime, i.e. $Re \leq 1$. Therefore, many authors developed experimental formulas for more general shapes, roughnesses, and velocity regimes, see e.g. Hallermeier (1981), Dietrich (1982), Van Rijn (1993), Cheng (1997), and Ferguson and Church (2004). In the following, a semi-empirical formula presented by Ferguson and Church (2004) is used which reads as

$$w_g = \frac{(\rho_s - \rho_f)/\rho_f \cdot g \cdot d_s^2}{C_1 \nu + \sqrt{0.75 \cdot C_2 \cdot (\rho_s - \rho_f)/\rho_f \cdot g \cdot d_s^3}}. \tag{10}$$

This model is an extension of Stokes' law and was fitted to real experimental data from Raudkivi (1998) and Hallermeier (1981). The second constant C_2 is an asymptotic value for the drag coefficient of the particle. Furthermore, experiments showed that C_2 can range from 0.4 to 1.2 for shapes varying from spherical to naturally shaped particles. Equation (10) was tested for different combinations of both constants and in regimes for a higher Reynolds number, i.e. $Re \geq 1000$. For natural sand grains Ferguson and Church (2004) suggested $C_1 = 18$ and $C_2 = 1.0$ but also hint at a maximum limit of $C_1 = 24$ and $C_2 = 1.2$ for extremely angular grains. With this approach the gravitational velocity is constant in the whole fluid domain and the term $\frac{\partial(w_g c)}{\partial x_2}$ reduces to $w_g \frac{\partial c}{\partial x_2}$ as presented in equation (7a).

2.5. Interchange between bed load and suspension load

In the complete sediment transport model the masses have to be conserved during the interchange between the bed load and the suspension load depending on the velocity. This interchange is modelled as a source term, i.e. a sink term, in the bed level model. All details of these terms will be discussed in the following. For the advection-diffusion equation (7a) the boundary conditions have to be thus modified properly.

The concept of a maximum concentration near the boundary is valid under the assumption that only the surplus mass Q_b can settle down from the fluid and this consequently results in a height difference h_{set} of the bedform. Vice versa the reference concentration prevails

as long as the sediment bed Ω_s is erodible. Thus, the Dirichlet boundary condition in equation (7c) results. Furthermore, it is common to add a source term in the concentration model for the mass flux S_b with the velocity v_n in normal direction. Consequently, the source and sink term for the model (7a) reads as

$$c = c_{ref} + \frac{S_b}{|v_n|} - Q_b \qquad\qquad \mathbf{x} \in \Gamma. \qquad (11a)$$

The source term $S_b/|v_n|$ is motivated by calculating the mass entrained into the suspension load by a velocity v_n normal to the boundary Γ. A modified approach for the flux from the sediment bed into the concentration model proposed by Malcherek (2004) is used here, which reads as

$$S_b = M \cdot \max(\tau - \tau_c, 0) \frac{\tau}{(\rho_s - \rho_f)gd} \qquad (12)$$

where $M = 2.2 \cdot 10^{-3} s/m$ denotes an empirical material parameter. Therefore, a mass which is set as an source term in the suspension model causes a height loss in the bed level model. This source term is only active if the shear stress τ is bigger than the critical shear stress τ_c. The reverse direction is modelled from the idea that a maximum reference concentration c_{ref} has adjusted in the layer near the boundary. Consequently, the sink term Q_b for the suspension model is defined as

$$Q_b = \max(c(\mathbf{x}, t) - c_{ref}, 0). \qquad (13)$$

If the difference between the ambient concentration $c(\mathbf{x}, t)$ and the reference concentration is positive, the height difference h_{set} for the bed level equation due to settled or entrained sediment results from the calculation

$$h_{set} = Q_b \cdot dx_1 \cdot dx_2 \cdot dx_3/(\rho_s \cdot dx_1 \cdot dx_3) = Q_b \cdot dx_2/\rho_s, \qquad (14)$$

where the control volume is calculated by $dx_1 \cdot dx_2 \cdot dx_3$.
In summary, an advection-diffusion equation is used to model the transport of the concentration of suspended material. This advection- diffusion model is equipped with Neumann boundary conditions at the non-sediment boundaries and modified Dirichlet boundary conditions including sink and source terms at the sediment boundary. Within this model the interchange between both transport stages is realised and the bed load and the suspension load can interact properly. An empirically derived diffusion coefficient K, the modelling of the settling velocity w_g, and the empirical mass flux S_b reflect the empirical influence in this model which has to be taken into account for the simulation of the transport process.

2.6. Slope stability and critical angle of repose

Granular media like sand or silt have the property that unstable slopes are formed, if piled up. This instabiltity causes the surplus masses to slide down the pile until a stable slope angle α_c establishes. This characteristic critical slope angle is influenced by different parameters, like shape, grain size, cohesion, moisture, and their interaction. This aspect needs to be reflected in a numerical model as well. Table 1 summarises some slope angles for different sediment types collected from the literature (Julien, 1995). To take this effect into account, we use the slope limiter algorithm presented in Burkow and Griebel (2016). Here, an iterative scheme is used to redistribute surplus masses and to limit the angle of the slope. In detail, if a slope angle $\alpha = \arctan(\|\nabla h\|_2)$ is larger than the critical angle

of repose α_c, the surplus mass is transferred to the neighbouring cells. Here, weights are introduced to distribute the masses equally. For the facing neighbours in the north, south, west, and east a weight $\omega_{n,s,w,e} = 1/6$ and for the diagonal neighbours $\omega_d = 1/12$ are chosen. Iterating over this scheme results in a new surface h_{α_c}, which obeys all angles, compare Burkow and Griebel (2016).

Table 1: Selection of values for the critical angle of repose α_c (Möller et al. (2002), Julien (1995)). The large variability of the material properties and the measuring of the values under water allows only rough estimates. This fact has to be taken into consideration when validating the numerical experiments.

Size	Properties	Angle of repose
Sand	dry to wet	$20 - -45°$
Gravel	roundness	$30 - -50°$
Silt & clay	shape and roughness	$20 - -60°$

2.7. Full fluid sediment model

In summary, all aspects of the fluid sediment interaction are now covered. The full model reads as

$$\frac{\partial \mathbf{u}}{\partial t} + \nabla \cdot (\mathbf{u} \otimes \mathbf{u}) = \frac{1}{Fr}\tilde{\mathbf{g}} - \nabla p + \frac{1}{Re}\Delta \mathbf{u} \qquad \text{on} \quad \Omega_f \in \mathbb{R}^3, \qquad (15a)$$

$$\nabla \cdot \mathbf{u} = 0 \qquad \text{on} \quad \Omega_f \in \mathbb{R}^3, \qquad (15b)$$

$$\frac{\partial h}{\partial t} = -\nabla \cdot \mathbf{q_s}(\tau(\mathbf{u})) + Q_b + S_b \qquad \text{on } P \qquad (15c)$$

$$\frac{\partial c}{\partial t} + \mathbf{u} \cdot \nabla c + w_g \frac{\partial c}{\partial x_2} - K\Delta c = 0 \qquad \text{on } \Omega_f. \qquad (15d)$$

The aforementioned boundary conditions (12) and (13) are added to this model. Furthermore, a buoyancy term formulation is chosen in the momentum equation. By multiplying the gravity force terms g in the Navier Stokes equations with $(\rho_f + c)/\rho_f$ a Boussinesq approximation for a buoyancy term

$$\tilde{\mathbf{g}} = \frac{\rho_f + c}{\rho_f}\mathbf{g}. \qquad (16)$$

is incorporated into the Navier Stokes equations. This approximation was previously introduced by Boussinesq (1903) for temperature-driven currents which resulted from density differences due to temperature differences. The Boussinesq approximation assumes only small differences between the density $\tilde{\rho}$ and the original density ρ_f, which is also a valid assumption for the suspended material.

3. Numerical aspects: Discretisation and Solver

For the numerical treatment of (15a) and (15b), we employ the three-dimensional parallel Navier-Stokes solver NaSt3D, see Griebel et al. (1998), with its recent improvements. NaSt3D is under development by the Institute for Numerical Simulation at the University of Bonn. It features finite differences schemes on staggered grids for the convective terms, like VONOS, ENO and WENO of up to fifth order for spatial derivatives in combination with second and third order time discretisation schemes, like Adams-Bashforth and

Runge-Kutta, compare Croce (2002). The size of the time step is adaptively determined to fulfill a CFL condition, which is used for the whole spatial domain. Moreover, it uses the projection approach by Chorin (1967), which reduces the equations (15a) and (15b) in each time step to a Poisson problem. This Poisson problem is solved with a BiCG-Stab solver. After the correction of the projected velocities with ∇p a divergence-free velocity field is achieved, which enforces the incompressibility condition of the fluid. Domain decomposition with ghost cells is applied to parallelise the algorithm. For further information see Croce (2002), Croce et al. (2009), and Adelsberger et al. (2014). Griebel and Klitz (2013) and Griebel and Rüttgers (2014) studied the parallel performance of the code and achieved nearly optimal scale up and speed up.

3.1. Exner's bed level equation

The bed level equation and the transport equation are discretised on the same staggered grid as for the Navier Stokes equations. The height h is approximated at the cell centres and the sediment fluxes $\mathbf{q_s}$ are situated on the faces of the cells. With this setting the finite differences schemes from the fluid solver are easily applicable. The spatial schemes are restricted to a two-dimensional setting. To this end, there are schemes like donor cell (DC), SMART, QUICK, or VONOS available. Moreover, an Adams-Bashforth second order (AB2) time stepping method is applied. For a detailed description of the applied schemes implemented in the setting in NaSt3D compare Griebel et al. (1998) and Croce (2002).

Whenever Ω_f changes in time, we have to update the fluid domain to couple the Navier–Stokes equations (15a) and (15b) with the Exner equation (15c) and the suspension model (15d). Here, a loosely partitioned coupled approach is used, which couples the fluid solver on a given fluid domain with the bed level equation. As a time step restriction for the Adams-Bashforth scheme a CFL condition is used, such that

$$dt \leq \frac{2dx^2}{\max_{ij} \|q_s\|_2},$$

(17)

where dx is the spatial grid size for an equidistant grid. This combination provides a robust method for the bed level equation, which is second order in both, space and time, compare Deriaz (2012). The new sediment height h is then treated by the first order obstacle representation of NaSt3D, which is described in Griebel et al. (1998).

3.2. Suspension load model

As already mentioned in Section (2.3), the suspension load model is a modified advection-diffusion equation with an additional settling term. For its discretisation, the techniques from our Navier Stokes solver are again applicable. To this end, the full spectrum of the convective schemes from NaSt3D can be used for the advection term. Moreover, the diffusion term is discretised by the standard Laplacian for scalars. Again, the staggered grid is employed in full three dimensions. Thus, the scalar concentration c is situated in the cell centre, whereas the advection velocity u and the gravitational settling velocity w_g are located at the cell faces. Furthermore, the second order explicit Adams-Bashforth scheme is applied for the time discretisation. This leads to the typical time step restriction for an advection-diffusion equation extended by the time step induced by the gravitational settling velocity w_g, i.e.

$$dt = \min \left(dt_{adv}, dt_{diff}, dt_{w_g} \right).$$

(18)

Here,

$$dt_{adv} \leq \frac{dx}{\max_{ij} \|\mathbf{u}\|_2} \qquad \text{and} \qquad dt_{w_g} \leq \frac{dx}{\max_{ij} \|w_g\|_2} \tag{19}$$

denote the CFL condition for the advection term and for the additional settling term, respectively. The diffusive CFL condition with the diffusion coefficient K is denoted by

$$dt_{diff} \leq \frac{dx^2}{6K}. \tag{20}$$

Note that the time step restriction arising from the advection term dt_{adv} is the same as the CFL condition for the fluid velocity $\mathbf{u}$ from the Navier Stokes solver NaSt3D, compare Griebel et al. (1998).

3.3. Algorithm and loosely coupling

Altogether, the coupling in each time step is realised as follows. First, the Navier-Stokes equations are solved on a given domain Ω_f. Second the computed velocity $\mathbf{u}$, the shear stress, the transport, and the new sediment height h_{α_c} are computed. Simultaneously, the advection-diffusion equation model is solved to compute the new suspension concentration c. Both, the sediment height and the concentration are used in the next time to determine the new domain Ω_f and the buoyancy term $\tilde{\mathbf{g}}$ in the Navier-Stokes equations. Finally, the sink and the source term for the Exner model as well as for the advection-diffusion model are computed for the next time step.

Overall, the loosely partitioned coupling algorithm reads as follows:

1. Computation of fluid properties (NaSt3D) (15a, 15b)
2. Computation of the shear stress τ and transport $\mathbf{q}_s$
3. Solution of Exner's equation (15c)
4. Solution of the suspension load model (15d)
5. Limiting the local slope angles iteratively
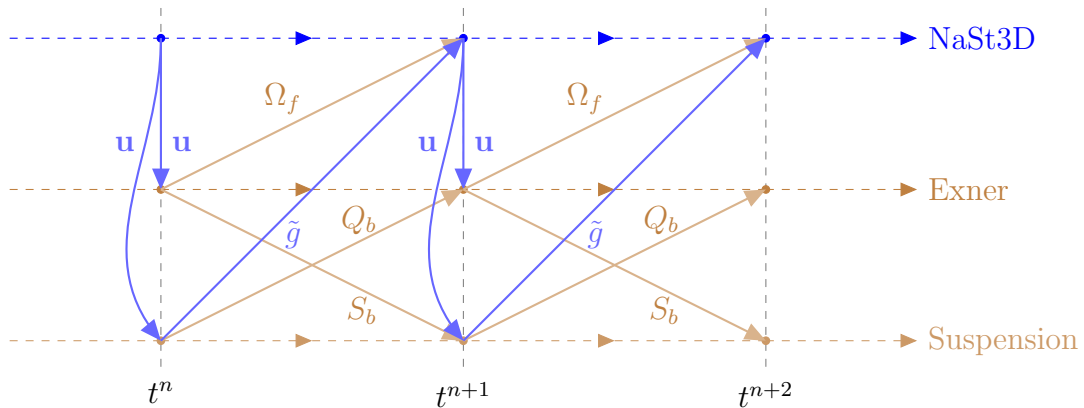6. Mapping the new h_{α_c} to geometry and adapting computational grid

Figure 2: Flow chart of our loosely partitioned coupling algorithm in each time step. The velocities from NaSt3D are used to compute the new sediment height h, which, after correcting to h_{α_c} due to the slope limiter iteration, determines the new Ω_f and therefore the new fluid domain.

A schematic view of the overall coupling is presented in Figure 2. Numerical tests concerning the numerical convergence for the sediment surface in this setting were previously performed in Burkow and Griebel (2016). There, a first order convergence for the sediment surface h was observed.

9

Table 2: Computational parameters and setting for the numerical simulation of a barchanoid dune presented in Figure 3.

NaSt3D					
Dimensions	Tfin	Re	PoissonSolver	it_{max}	ε
$20.0 \times 5.0 \times 10.0$	250	1000	BiCGStab	1000	10^{-8}

Exner + Suspension					
Transp.Formula	τ_c	d_{50}	d_s	α_c	K
Meyer-Peter-M.	0.047	$2\,mm$	$0.01\,mm$	$40°$	0

NaSt3D		Exner		Suspension	
spatial	temporal	spatial	temporal	spatial	temporal
QUICK	AB2	DC	AB2	DC	AB2

4. Numerical results: The temporal evolution of a Barchanoid dune

In the following, the full model is applied to the simulation of a barchanoid dune evolving from a symmetric pile of sand.

4.1. Experimental setting

The basic setting for this example is to use a channel with $20\,m \times 5\,m \times 10\,m$ and a spatial resolution of $200 \times 50 \times 100$, which results in a spatial grid size of $dx = 0.1\,m$. On the left inflow face a velocity of $u = 5\,m/s$ is set. A backward facing step is placed at the inflow to avoid an unintended and uncontrollable sediment movement during the initial phase of the simulation. At the right face a Neumann condition is employed. All other walls are modelled as frictionless surfaces by imposing slip boundary conditions. We assume fluid viscosity of $\nu = 10^{-5}m^2/s$. For theinitial configuration a sand layer of $1\,m$ is chosen for the sediment surface and a laterally extended conical pile of sand is placed on top of it. Here, the pile acts as the bed base material from which the dune develops. The top of this pile reaches up to $3.35\,m$. Before the start of the simulation the slope limiter algorithm is applied to ensure that the slope angle of the pile is below the critical angle of repose ($\alpha_c = 40°$). The particle size for the bed load transport is $d_{50} = 0.002\,m$ and for the suspension load $d_s = 0.00001\,m$. For the bed load transport the Meyer-Peter and Müller formula from Section (2.2) is used with $\tau_c = 0.047$. Furthermore, a reference concentration in the suspension load model of $c_{ref} = 2.0 \cdot 10^{-5}kg/l$ is chosen. In this large scale example, the diffusion of the suspension load is neglected, i.e. $K = 0$, and thus solely transport is considered. To compute the Reynolds Number Re a reference length of $l = 0.002$ is used. This corresponds to the particle size d_{50}. For the linear solver a BiCGStab is chosen, which iterates until the residual is less than $\varepsilon = 10^{-8}$. The employed parameters and further information on the initial data and our numerical method are given in Table 2 and in Figure 3. For the computation of our numerical results, we used a HPC cluster, which has 5 Dell PowerEdge R910 computing nodes with 160 Intel Xeon X7560 2.226 GHz CPU cores and a main memory of 2560 GB in total, i.e. one computing node contains 32 CPU cores and has 512 GB main memory. Moreover a Mellanox ConnectX Infiniband realises the MPI communication. A Linpack performance test of the system resulted in 1349 GFlops/s with a parallel efficiency of 93%. The computational time for our experiment was $144\,h$.

4.2. Evaluation and discussion of the numerical result

In Figure 4 the result of our simulation after $250\,s$ is presented. The morphology of a barchanoid dune is obtained, i.e. the whole dune body is crescent-shaped and the luvside
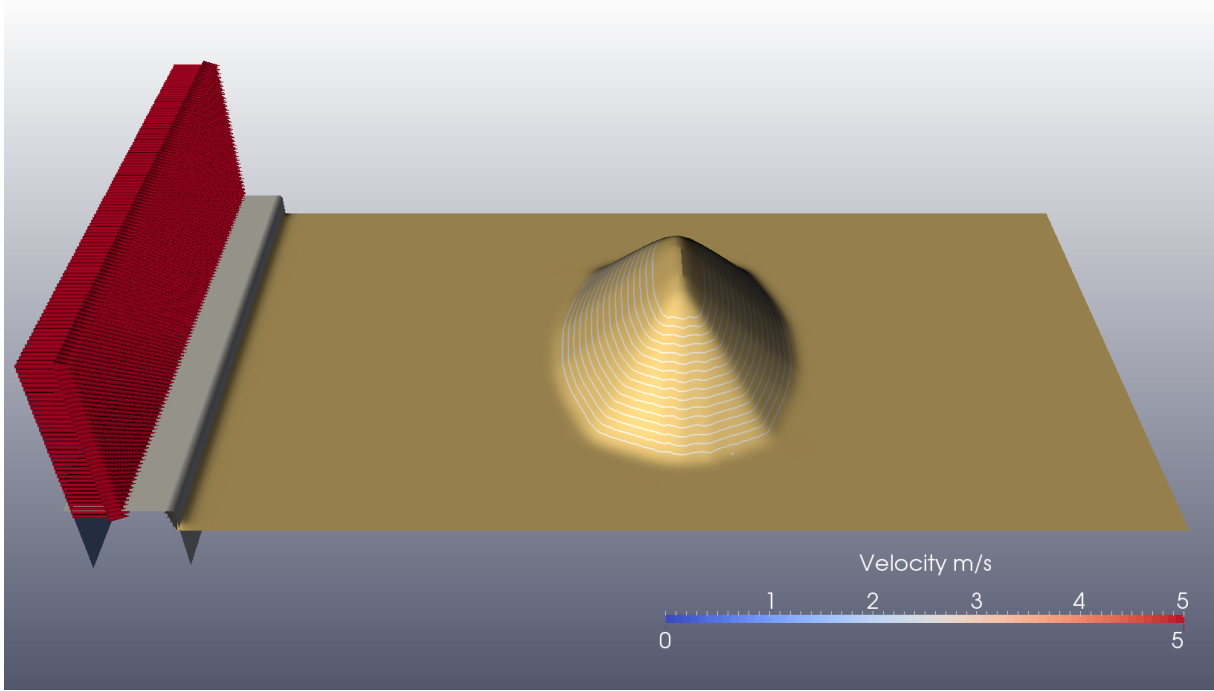
Figure 3: The starting configuration for the simulation of the development of the barchanoid dune. Flow direction is from the left to the right and a constant velocity $u = 5\,m/s$ is set at the left wall. In the middle of the channel there is an initial laterally elongated sediment pile which is transported over time and forms the dune in the channel ($20\,m \times 5\,m \times 10\,m$).

of the body is sloping upwards, whereas the leeside is dominated by the angle of repose. In detail, the flow transports the particles over the dune body. After reaching the crest of the dune, the particles slide down the lee slope and form the specific angle of repose. Additionally, the lateral parts of the dune body, the horns, advance faster than the inner parts, which results in the typical crescent shape with preceding dune horns. Due to the uniform inflow profile in this example a barchanoid dune indeed develops.

The evolution of the dune from the initial pile of sand is demonstrated in Figure 5. Here, the transition from a pile with symmetric slopes to a crescent-shaped dune is clearly seen. The initial forming of the lateral horns is caused by the uniform velocity profile. A steady bed transport leads to an asymmetric cross section of the dune body with a slightly increasing luvslope and a leeslope limited by the angle of repose. Additionally, the asymmetric cross profile of the dune is also well recovered.

Moreover, in Figure 5 the suspension load transport over time is additionally visualised on a cross section in the middle of the domain. Furthermore, the suspension load and the velocities are given on this cross section. The erosion of the material from the sediment surface and the entrainment into suspension starts at the crest of the dune. At this point the shear stress surpasses the critical value first, and therefore the material is eroded and transported into the fluid body. At later times the interaction of the flow with the sediment surface and the suspended material gets more complicated and becomes multi-layered. On the one hand, the flow forms the moving sediment surface into a barchanoid dune. On the other hand, the erosion of the material from the surface into the suspension load interacts with the flow by the gravitational source term coupled by the Boussinesq approximation.

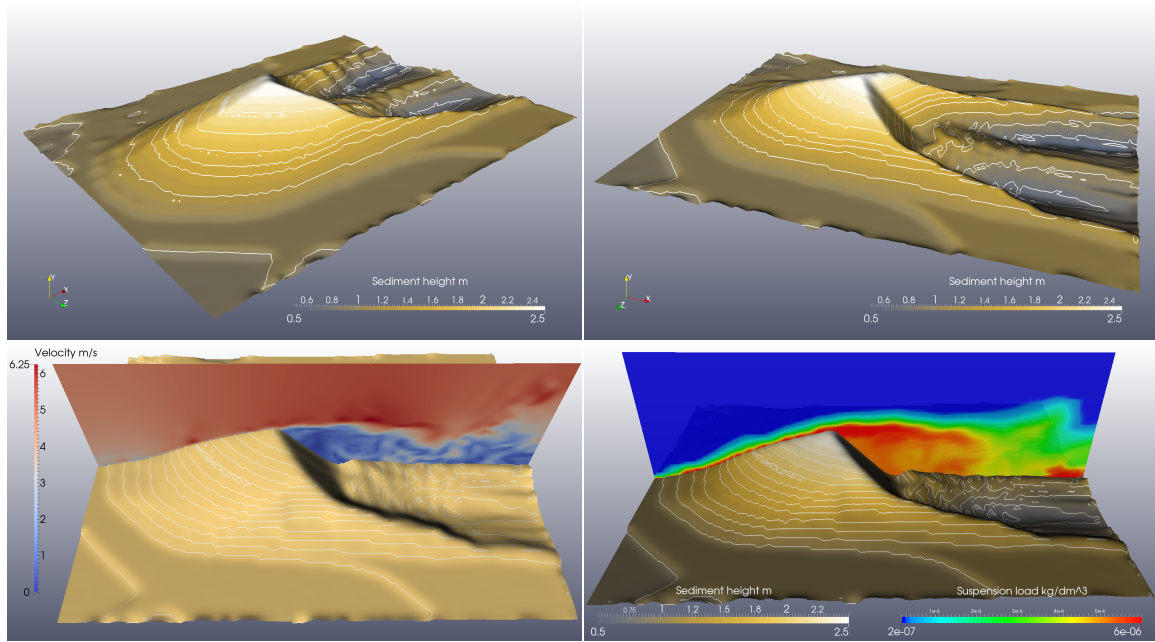In Figure 6 we depict the recirculation zone behind the dune in detail. In this recircula-

11

Figure 4: Top: Visualisation of two perspectives of the final sediment surface ($250\,s$) with height isocontours indicating equal height levels. The typical crescent shape is well reproduced. Bottom: Illustration of the velocity field on a cross section through the middle of the domain (left). Visualisation of the suspended material on the same cross section as for the velocities (right). Here, the recirculation zone behind the dune can be seen.

tion zone the transport capacity is high enough and sufficiently moderate to carry some suspended material with the flow. When the velocities are high, the suspension load is transported away. In contrast, in zones where the velocity and the transport capacity decrease, e.g. in the wake of the dune, the suspension load is dispensed all over the fluid, compare Figure 5.

The movement of natural dunes and their build-up is in the temporal range of days and weeks. Due to computational limitations we can only give a qualitative comparison of our simulated dune prototype with real dunes. Nevertheless, this comparison confirms the realism of our simulated results, compare Figure 7. Here, the crescent shape and the trailing horns are well recovered. From the visualised suspension load near the dune it can be seen that the transport processes are in good agreement with the observations from field experiments, compare Sauermann et al. (2000), Sauermann et al. (2001), and Schwämmle and Herrmann (2003). Especially the temporal evolution follows the observation from field experiments. The comparison of the suspension load blasting from the crest with that from a field example qualitatively confirms the numerical simulation.
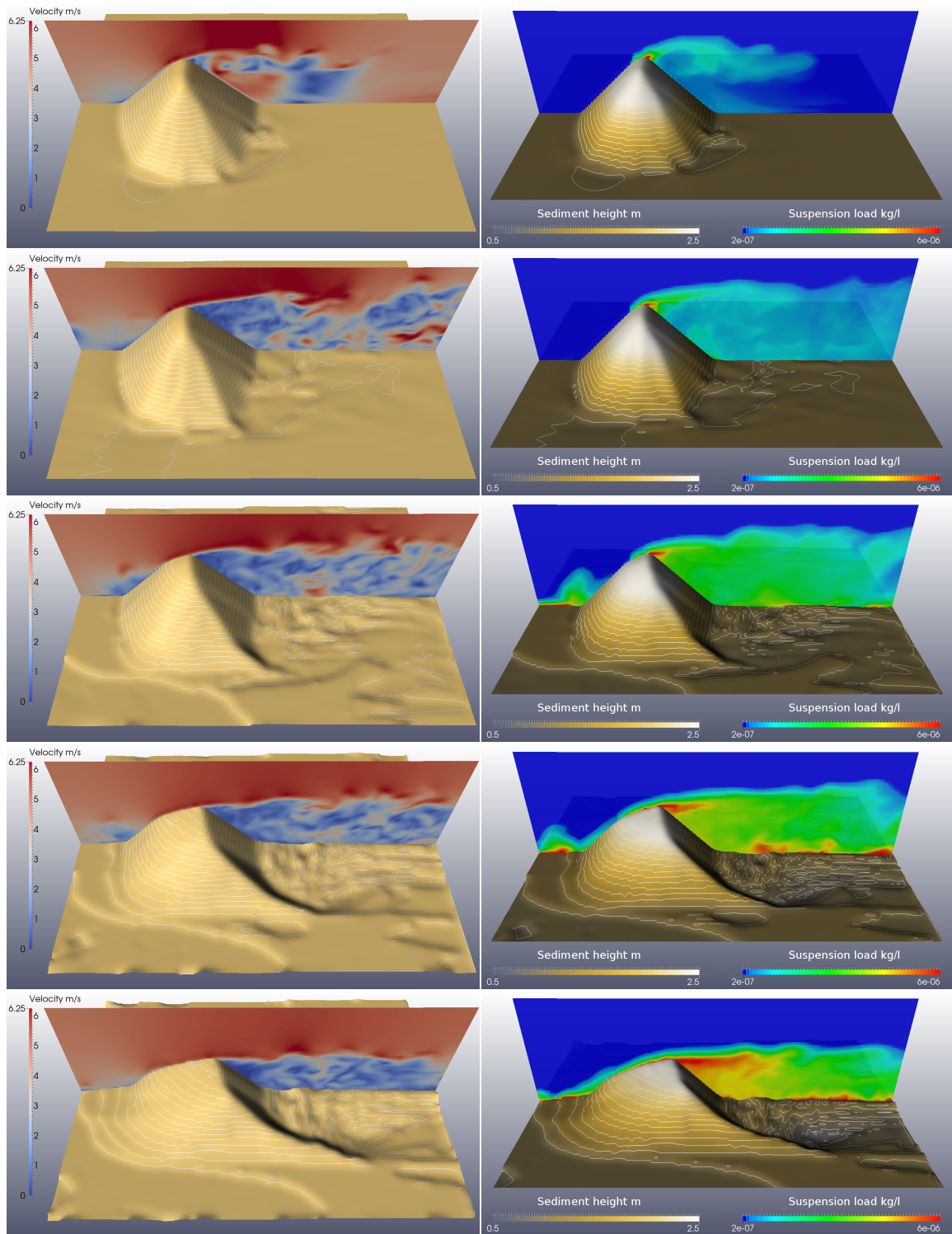
Figure 5: Temporal evolution of the flow field (left) and suspension load (right) at the time steps $t = \{2\,s, 5\,s, 25\,s, 75\,s, 150\,s\}$. The visualisation of the dune surface is enhanced by isocontours for the height in both sequences.
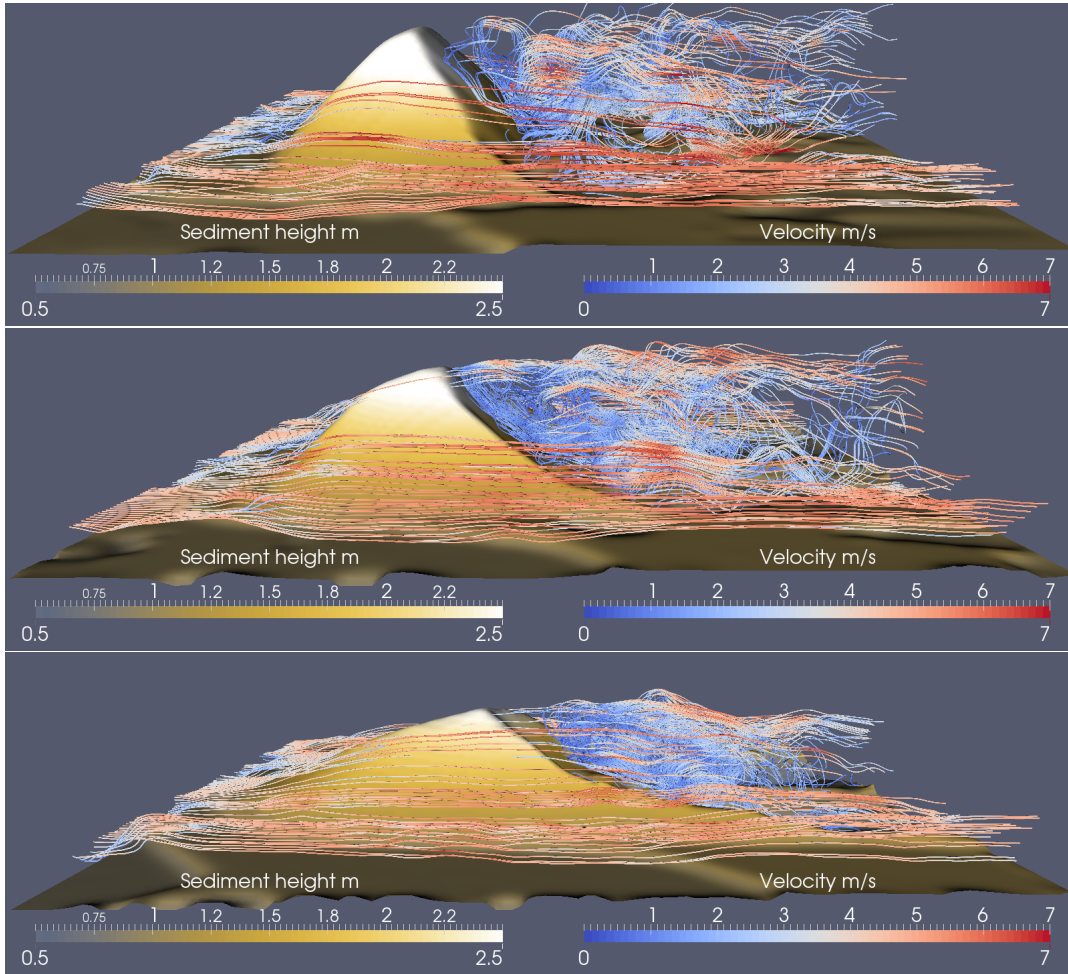
Figure 6: The recirculation zone and the vortex system behind the dune at the time steps $t = \{20\,s, 83.5\,s, 250\,s\}$.

Figure 8 presents four cross profiles of a classical dune from Groh et al. (2009) and four cross profiles from our numerical simulation. Both experimental assemblies start at the beginning with a symmetric pile of sand with identical leeside and luvside slope angles. This symmetric sand body is transformed into an asymmetric dune body with a slightly increasing luvside and a steep leeside slope. Our simulation of a prototype dune reproduces the formation of the asymmetric shape over time. Despite the fact that the numerical setting is different in size and physical time compared to the experimental data, the basic features of the real experiments are recovered and comparable. A further quantitative direct comparison in this case is not possible due to computational limitations.
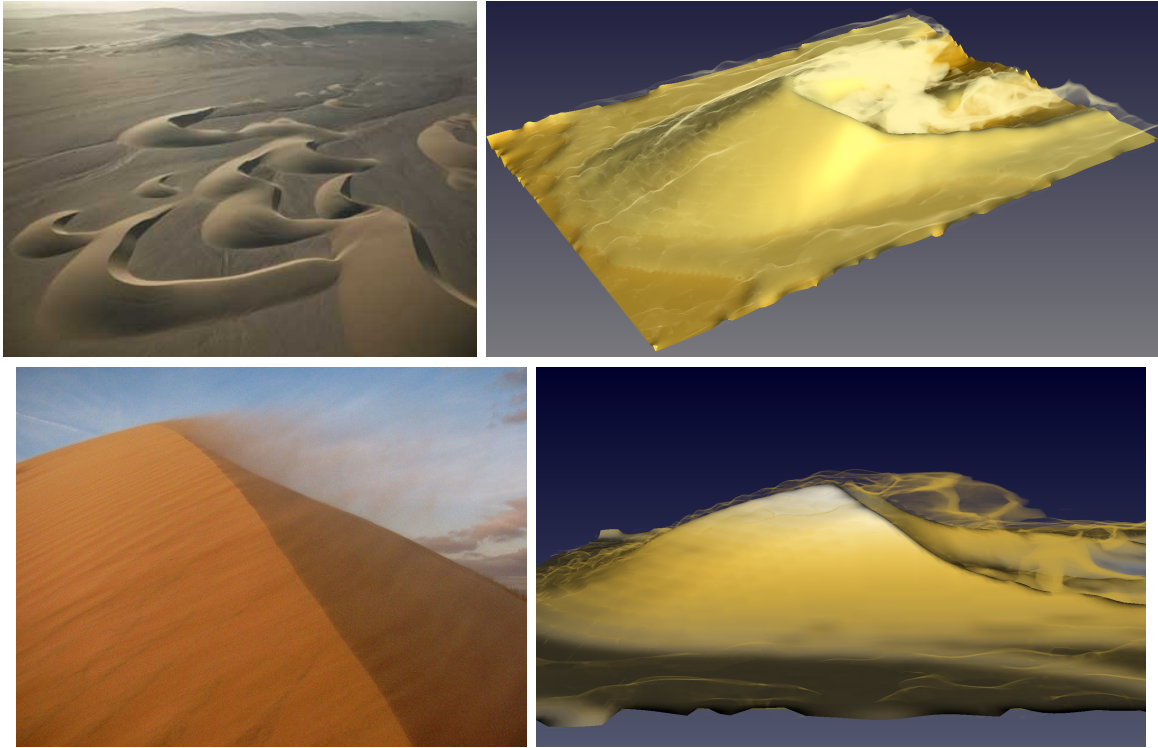
Figure 7: Top: A qualitative comparison between a barchanoid dune from a dune field in Namibia (Flood, undated) (left) and the simulated dune (right). Bottom: Sand blowing off a real (Destefano, 2011) (left) and a simulated (right) dune crest.
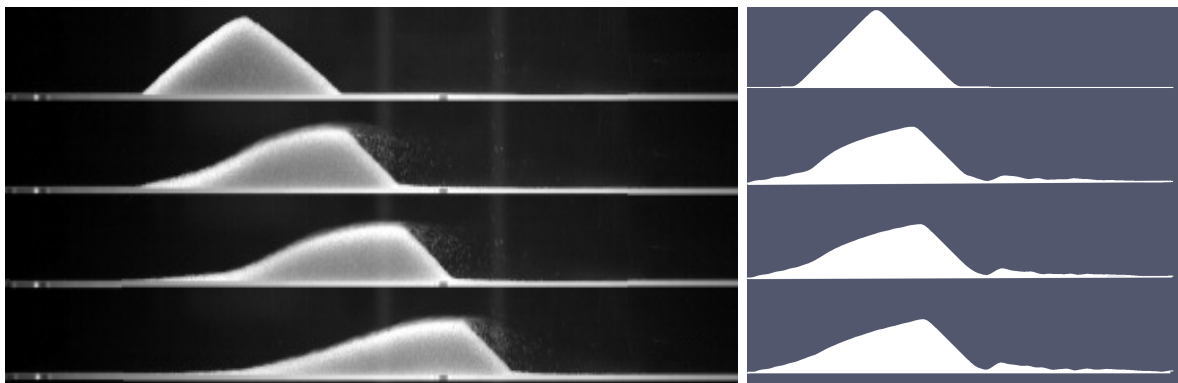

Figure 8: Lateral view of a dune profile from an experiment conducted by (Groh et al., 2009) (top) and our numerical simulation (bottom). In both experiments the dune evolves from an initially symmetric pile of sand over time. The classical dune geometry is visible. The leeside is limited by the angle of repose and the luvside increases slightly.
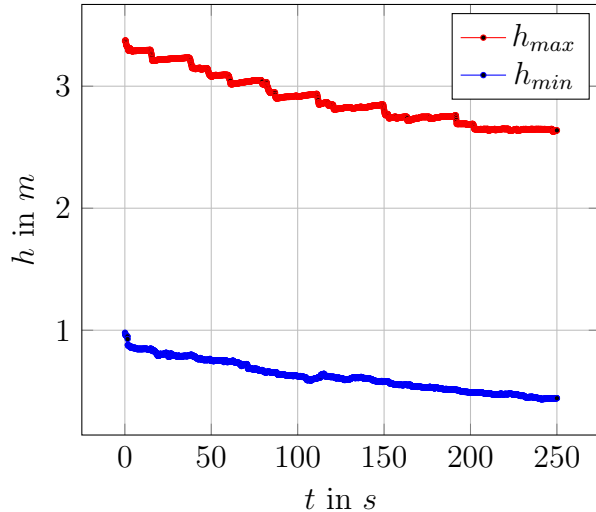
Figure 9: Temporal development of the minimum and maximum sediment height in the simulation. The maximum denotes the height of the dune crest. Kinks in the plot are caused by abrupt slope correction by the slope limiter to ensure the angle of repose. In contrast, a constantly smooth erosion of the sediment bed is denoted by the minimum.

Figure 9 shows the maximum and minimum height over time. In both plots a decrease is visible. The maximum denotes the crest height of the dune. There are several kinks in the plots with a previous slight increase in the height. This behaviour can be explained by the sediment transported upwards the dune which slides abruptly down when the critical angle of repose is surpassed and the slope limiter corrects the slopes.

5. Conclusion

We presented a fully coupled three-dimensional fluid sediment model for current-driven sediment processes and applied it to the temporal evolution of a barchanoid dune from a symmetric pile of sand. Exner's bed level equation, the suspension load model, and the Navier–Stokes equations were discretised with a finite difference approach on a staggered grid. A slope limiting iterative process was used to secure the slope angles of the sediment. We applied a donor cell scheme in space and an Adams Bashforth discretisation scheme in time. All equations were treated explicitly in each time step with a loosely coupled overall algorithm, which resulted in an additional CFL condition. With this algorithm, we computed the three-dimensional evolution of a dune. Our numerical simulation reproduced the typical transport processes which lead to a classical barchanoid dune body. The shape, the geometry, and the vortex systems were well recovered. The transport of the suspended material as well as the morphological changes are sufficiently resolved. Moreover the maximum and minimum height of the sediment surface were investigated over time. These results were qualitatively in good agreement with data in the literature. Altogether, our new fully coupled numerical approach showed the ability to reproduce the evolution of a dune. This promises to also simulate the complex transport processes leading to the formation of various other bedforms in future experiments. In a comparative study of numerical simulations and real experiments a turbulence approach like in Burkow and Griebel (2016) would be a possible extension of our model.

6. References

Adelsberger, J., Esser, P., Griebel, M., Groß, S., Klitz, M., Rüttgers, A., 2014. 3D incompressible two-phase flow benchmark computations for rising droplets. In: Proceedings of the 11th World Congress on Computational Mechanics (WCCM XI), Barcelona, Spain.

Boussinesq, J., 1903. Theorie analytique de la chaleur. Vol. 2. Gathier–Villars.

Burkow, M., Griebel, M., 2016. A full three dimensional numerical simulation of the sediment transport and the scouring at a rectangular obstacle. Computers & Fluids 125, 1–10.

Campos, R., 2001. Three-dimensional reservoir sedimentation model. Ph.D. thesis, University of Newcastle, Faculty of Engineering.

Chanson, H., 1999. The Hydraulics of Open Channel Flow - An Introduction. Edward Arnold, London.

Cheng, N., 1997. Simplified settling velocity formula for sediment particle. Journal of Hydraulic Engineering 123 (2), 149–152.

Chorin, A. J., 1967. A numerical method for solving incompressible viscous flow problems. Journal of Computational Physics 2 (1), 12–26.

Coleman, S. E., Nikora, V. I., 2009. Exner equation: A continuum approximation of a discrete granular system. Water Resource Research 45, 1–8.

Croce, R., 2002. Ein paralleler, dreidimensionaler Navier-Stokes-Löser für inkompressible Zweiphasenströmungen mit Oberflächenspannung, Hindernissen und dynamischen Kontaktflächen. Diplomarbeit, Insitut für Numerische Mathematik, Universität Bonn.

Croce, R., Griebel, M., Schweitzer, M. A., 2009. Numerical simulation of bubble and droplet-deformation by a level set approach with surface tension in three dimensions. International Journal for Numerical Methods in Fluids 62 (9), 963–993.

Daintith, J., 2009. A Dictionary of Physics. Oxford Paperback Reference. OUP Oxford.

Deriaz, E., 2012. Stability conditions for the numerical solution of convection-dominated problems with skew-symmetric discretizations. SIAM J. Numerical Analysis 50 (3), 1058–1085.

Destefano, L., 2011. http://gadling.com/tag/mojave-desert/.

Dietrich, W. E., 1982. Settling velocity of natural particles. Water Resour. Res. 18 (6), 1615–1626.

Doré, A., Bonneton, P., Marieu, V., Garlan, T., 2016. Numerical modeling of subaqueous sand dune morphodynamics. Journal of Geophysical Research: Earth Surface 121 (3), 565–587.

Exner, F. M., 1925. Über die Wechselwirkung zwischen Wasser und Geschiebe in Flüssen. Sitzungsbericht Akademie der Wisssenschaft Wien 134, 165–180.

Ferguson, R. I., Church, M., 2004. A simple universal equation for grain settling velocity. Journal of Sedimentary Research 74(6), 933–937.

Flood, S., undated. http://www.gettyimages.co.uk/detail/photo/namibia-skeleton-coast-sand-dunes-high-res-stock-photography/sb10067261u-001.

Giri, S., Shimizu, Y., 2006. Numerical computation of sand dune migration with free surface flow. Water Resources Research 42 (10).

Goudie, A., 2014. Physische Geographie: Eine Einführung. Vol. 4. Springer Berlin Heidelberg.

Griebel, M., Dornseifer, T., Neunhoeffer, T., 1998. Numerical Simulation in Fluid Dynamics, a Practical Introduction. SIAM, Philadelphia.

Griebel, M., Klitz, M., 2013. Simulation of droplet impact with dynamic contact angle boundary conditions. In: Singular Phenomena and Scaling in Mathematical Models. Springer International Publishing Switzerland, pp. 297–325.

Griebel, M., Rüttgers, A., 2014. Simulation of dilute polymeric fluids in a three-dimensional contraction using a multiscale FENE model. Vol. 1593 of AIP Conference Proceedings. pp. 539–543, proceedings of PPS-29: The 29th International Conference of the Polymer Processing Society, Nuremberg, Germany.

Groh, C., Rehberg, I., Kruelle, C. A., 2009. How attractive is a barchan dune? New Journal of Physics 11 (2), 023014.

Hallermeier, R. J., 1981. Terminal settling velocity of commonly occurring sand grains. Sedimentology 28, 859–865.

James, S. C., Jones, C. A., Grace, M. D., Roberts, J. D., 2010. Advances in sediment transport modelling. Journal of Hydraulic Research 48 (6), 754–763.

Julien, P., 1995. Erosion and Sedimentation. Cambridge University Press, Cambridge.

Kantoush, S. A., Bollaert, E., Schleiss, A. J., 2008. Experimental and numerical modelling of sedimentation in a rectangular shallow basin. International Journal of Sediment Research 23 (3), 212–232.

Khosronejad, A., Kang, S., Sotiropoulos, F., 2012. Experimental and computational investigation of local scour around bridge piers. Advances in Water Resources 37 (0), 73–85.

Kubatko, E. J., Westerink, J. J., 2007. Exact discontinuous solutions of Exner's bed evolution model: Simple theory for sediment bores. Journal of hydraulic engineering 133 (3), 305–311.

Kubatko, E. T., Westerink, J. J., Dawson, C., 2006. An unstructured grid morphodynamic model with a discontinuous Galerkin method for bed evolution. Ocean Modelling 15, 71–89.

Malcherek, A., 2004. Sedimenttransport und Morphodynamik. Lecture Notes, Universität der Bundeswehr, Institut für Wasserwesen, München.

Marek, M., 2001. Simulation des Sedimenttransports in Suspension und als Geschiebe - Ein Vergleich für das Jade-Weser-Astuar. Master's thesis, Institut für Wasserwirtschaft und Kulturtechnik, Universität Karlsruhe.

Meyer-Peter, E., Müller, R., 1948. Formulas for bed-load transport. In: Proceedings of the 2nd Meeting of the International Association for Hydraulic Structures Research. IAHR, Stockholm, Sweden, pp. 39–64.

Möller, L. E., Kuhlman, K. R., Marshall, J. R., Towner, M. C., 2002. The snoopy angle of repose experiment: Calibration of an instrument to determine the angle of repose of Martian dust. Lunar and Planetary Science 33.

Nabi, M., de Vriend, H. J., Mosselman, E., Sloff, C. J., Shimizu, Y., 2013. Detailed simulation of morphodynamics: 3. ripples and dunes. Water Resources Research 49 (9), 5930–5943.

Officer, C. B., 1982. Fluid and material diffusion coefficient determinations from sediment cores. Estuarine, Coastal and Shelf Science 14 (4), 459–464.

Paola, C., Voller, V., 2005. A generalized Exner equation for sediment mass balance. Journal of Geophysical Research: Earth Surface 110 (F4).

Parker, G., 2004. 1D Sediment Transport Morphodynamics with Applications to Rivers and Turbidity Currents. E-Book, http://hydrolab.illinois.edu/people/parkerg/morphodynamics-e-book.htm.

Raudkivi, A., 1998. Loose Boundary Hydraulics. Taylor & Francis.

Razmi, A., Firoozabadi, B., Ahmadi, G., 2009. Experimental and numerical approach to enlargement of performance of primary settling tanks. Journal of Applied Fluid Mechanics 2 No. 1, 1–12.

Sauermann, G., Kroy, K., Herrmann, H. J., 2001. Continuum saltation model for sand dunes. Phys. Rev. E 64, 031305.

Sauermann, G., Rognon, P., Poliakov, A., Herrmann, H., 2000. The shape of the Barchan dunes of southern Morocco. Geomorphology 36 (1-2), 47–62.

Schwämmle, V., Herrmann, H. J., 2003. Modelling transverse dunes. arXiv:cond-mat/0301589v1.

Sedimentation & River Hydraulics Group, November 2006. Erosion and Sedimentation Manual. U.S. Department of the Interior Bureau of Reclamation, Denver, Colorado.

Van Rijn, L. C., 1993. Principles of sediment transport in rivers, estuaries and coastal seas. Vol. 1006. Aqua publications Amsterdam.

Wong, M., Parker, G., 2006. Reanalysis and correction of bed-load relation of Meyer-Peter and Müller using their own database. Journal of Hydraulic Engineering 132, 1159–1168.

Wu, W., Shields, F. D., Bennett, S. J., Wang, S. S. Y., 2005. A depth-averaged two-dimensional model for flow, sediment transport, and bed topography in curved channels with riparian vegetation. Water Resources Research 41 (3).

Yoon, J.-Y., Kang, S.-K., 2005. A numerical model of sediment-laden turbulent flow in an open channel. Canadian Journal Civil Engineering 32, 233–240.